Desalination and Water Treatment
www.deswater.com

doi: 10.1080/19443994.2016.1182078

57 (2016) 28284–28293
December

Taylor & Francis
Taylor & Francis Group

Hexavalent chromium adsorption from aqueous solutions using nanoporous graphene/Fe_3O_4 (NPG/Fe_3O_4: modeling and optimization)

Sanaz Fathi[a], Roshanak Rezaei Kalantary[b,*], Alimorad Rashidi[c], Abdolreza Karbassi[d]

[a]*Faculty of Environment and Energy, Department of Environmental Science, Tehran Science and Research Branch, Islamic Azad University, Tehran, Iran, Tel.+98 2144099430; Fax: +98 21 44712435; email: sanazfathi2@gmail.com*
[b]*Research Center for Environmental Health Technology (RCEHT), Iran University of Medical Sciences, Tehran, Iran, email: rezaei.r@iums.ac.ir*
[c]*Nanotechnology Research Center, Research Institute of Petroleum Industry (RIPI), Tehran, Iran, email: rashidiam@gmail.com*
[d]*Graduate Faculty of Environment, University of Tehran, P.O. Box 14155-6135, Tehran, Iran, email: akarbasi@ut.ac.ir*

Received 29 December 2015; Accepted 18 April 2016

ABSTRACT

In the present study, nanoporous graphene was magnetized with Fe_3O_4 nanoparticles (NPG/Fe_3O_4) to promote its capabilities for the faster removal of hexavalent chromium (Cr(VI)) from aqueous solution. In order to minimize the adverse effects of magnetized nanoparticles, they can be easily separated by an external magnetic field. The size, crystallinity, and morphological structures of the adsorbent were characterized by SEM, TEM, XRD, and FT-IR techniques. The effect of various experimental parameters such as pH of solution, contact time, adsorbent dosage, temperature, and initial Cr(VI) concentrations on the adsorption efficiency was investigated in a batch procedure. The experimental equilibrium data were fitted to the Freundlich isotherm and pseudo-second-order kinetic models. According to thermodynamic studies, the adsorption process was spontaneous and endothermic in nature. Finally, our results suggested that NPG/Fe_3O_4 has a good potential in the Cr(VI) removal and can be effectively utilized in industrial wastewater treatment processes.

Keywords: Environment; Aquatic; Pollution; Metal; Nanoparticles; Magnetic

1. Introduction

Discharge of heavy metals into the environment, even at low levels, can bring about adverse effects on ecosystem. These pollutants can be further accumulated in the human and animal bodies [1]. Solubility and accumulation characteristics of hexavalent chromium (Cr(VI)) in the living organisms can also be irreversible [2]. It should be pointed out that Cr(VI) is a highly toxic metal that can be found in many industries such as textiles, printing inks, and leather [3]. Until now, various techniques have been applied to remove Cr(VI) from aqueous solutions, such as sedimentation [4], reduction [5], ultra-filtration [6], and adsorption [7]. Adsorption is now viewed as a superior technique for its cost-effectiveness and flexibility. Many organic and inorganic adsorbents such as activated carbon [8], graphene [9], purolite [10], chitosan [11], metal oxides [12], and biological wastes [13] have been used for wastewater treatment procedures so far. Graphene has extraordinary physical and electrical

*Corresponding author.

properties such as large surface area, open porous structure, flexibility, chemical stability, and very high electrical conductivity that warrant it as a good candidate for constructing graphene-based composite materials with metal oxides [14,15]. Nanoporous graphene (NPG) has been synthesized by precipitation chemical vapor (CVD) technique as modern separation systems and magnetite by nanoparticles of Fe_3O_4 powder (NPG/Fe_3O_4). This magnetization is a simple and effective method of particle separation along with pollutant removal from aqueous solution. These particles should be including nano-sized magnetic iron oxide. These magnetized materials can be easily recycled used *in situ*, and thus is suitable for online separation in industrial processes [16]. The separation of magnetized materials can be carried out by a simple hand magnet [17]. The presence of Fe_3O_4 in the structure of NPG may provide better kinetics for the adsorption of pollutants, due to small size and high surface-area-to-volume ratio [18]. In this study, NPG was synthesized and characterized by several techniques such as SEM, TEM, XRD, and FTIR. The NPG was applied for the Cr(VI) removal from aqueous solutions in the best conditions of solution pH, contact time, temperature, initial ion concentration, and adsorbent dosage. The adsorption equilibrium experiments were conducted then the experimental data were fitted to the best isotherm and kinetic models. The thermodynamic of adsorption was also investigated.

2. Materials and methods

2.1. Chemicals

Extra pure chemicals include anhydrous iron(III/II) chloride (99.9%) ammonia solution (28%) hydrazine hydrate were obtained from Merck, Co. Ultrapure water was used throughout the experiments. Potassium dichromate was used as a source of heavy metal. The pH of solutions was adjusted by adding 0.1 M hydrochloric acid (0.1 M HCl) and 0.1 M sodium hydroxide (0.1 M NaOH) solutions. The adsorbent was separated from the solution by a hand magnet (dimension, 5 cm × 4 cm × 4 cm; intensity, 1.3 T).

2.2. Synthesis of NPG

Precipitation CVD technique for the synthesis of NPG in large volumes and low cost is an effective method [19]. In this method, for direct synthesis of porous graphene, about 5 g naphthalene as a carbon source was put in a quartz reactor tube. Subsequently, it was subject to the rock wool separated carbon resource and catalyst. Catalyst consists of a copper foil in the reactor. Graphene is formed on the metals such as copper [20], nickel [21], etc. Copper is a better choice for the synthesis of graphene, due to its low cost and flexibility. Synthesis was carried out in a rapid thermal processing CVD chamber, fitted with a pressure regulation device and temperature control by an optical pyrometer [22]. Furthermore, the tube was put in the reactor and heated to reach a temperature of 1,000˚C for 1 h. By passing hydrogen gas during activated copper catalyst, graphene was formed on the copper surface [19]. In addition, for the synthesis of NPG, the produced graphene was stirred in 18% HCl solution for about 16 h at room temperature (25 ± 2˚C) and then washed with distilled water several times. Finally, the synthesized adsorbent was dried at 100˚C [23].

2.3. Synthesis of NPG/Fe_3O_4

NPG/Fe_3O_4 nanocomposite was synthesized according to the method reported by Juang et al. [24] with some modifications. First, 0.9 g of NPG was dissolved in 250 mL of distilled water using ultra-sonication for 2 h at 60˚C. Then, 10 g of $FeCl_3$ and 4 g of $FeCl_2$ were dissolved in 25 mL of distilled water and then exposed to N_2 gas for about 5–10 min. Subsequently, 50% (w/v) of NaOH solution was added dropwisingly to the mixture to adjust the solution pH at >12. The temperature of the solution was raised to 80˚C. The as-synthesized solid products were separated by a strong magnet then washed thoroughly with ultrapure water and absolute ethanol to remove any impurities. In the final step, it was dried in a vacuum oven at 50˚C for 24 h [25].

2.4. Characterization of the NPG/Fe_3O_4

Scanning electron microscopy (SEM, model MIRA3, Tescan, Czech Republic) was used to measure surface morphology, size, and distribution of synthesized composite. An X-ray diffraction instrument (XRD; model EDX, TESCA MIRA3, Czech Republic) with Cu-Kα radiation at 40 kV, 40 mA, and 25˚C was used to determine the crystalline characterizations of nanoparticles. The morphological features and shape of the adsorbent were recorded by transmission electron microscopy (TEM, model PHILIPS, EM 208 S) with 100 keV. The BET analysis (Quantachrome, 2000, NOVA) was applied to determine the specific surface area and volume of the pores of the adsorbent. Before the test, the sample was degassed at 100 Å for 8 h in an outgassing station to remove any adsorbed water or entrapped gases in the sample. The FT-IR spectrum

of synthesized composite was measured by a spectrophotometer (Tensor 27, Bruker, Germany). The latter was also employed to determine the functional groups on the surfaces of adsorbent.

2.5. Batch adsorption experiments

The stock solution (1,000 mg/L) of Cr(VI) was prepared by dissolving a certain amount of $K_2Cr_2O_7$ in 1,000 mL of deionized water. The pH of solution was adjusted by 0.1 M NaOH and 0.1 M HCl solutions. The effect of different experimental variables, such as pH of solution, contact time, different adsorbent dosages, temperature, and different initial ion concentrations on the adsorption efficiency was investigated. To ensure the perfect mixing of the adsorbent and dissolved Cr (VI), samples were put on a rotary shaker and then shaken vigorously at 200 rpm for about 60 min. Subsequently, adsorbents were magnetically separated from the solution using a hand magnet. The residual metal concentration in the solution was determined by an atomic absorption spectrophotometer (7400CE CECIL) at wavelength of 540 nm using the diphenylcarbazide colorimetric method. Finally, the adsorptive removal efficiency of Cr(VI) using NPG/Fe_3O_4 was calculated using the following equation:

$$R(\%) = \frac{C_0 - C_e}{C_0} \times 100 \quad (1)$$

where C_0 and C_e are the initial and residual concentrations of contaminant in solution (mg/L), respectively.

2.6. Isotherms, kinetics, and thermodynamics of adsorption

The Langmuir and Freundlich isotherm models were used to evaluate Cr(VI) adsorption onto the NPG/Fe_3O_4 surfaces. To facilitate adsorption process, isotherm models were obtained from the data derived from the regression analysis. The k_L (L/mg) is the empirical constant related to energy and q_m (mg/g) represents the maximum adsorption capacity. The k_F and n are the Freundlich constants related to the adsorption capacity and intensity that can be calculated from the slope and intercept of the plot of ln C_e against ln q_e, respectively. The q_m and k_L parameters are calculated from the slope and intercept of the plot of C_e/q_e against C_e, respectively. The chemical kinetics deals with the experimental conditions influencing the rate of a chemical reaction. Herein, two kinetic models including the pseudo-first-order and pseudo-second-order models were applied for the modeling of the adsorption of Cr(VI) on NPG/Fe_3O_4. Thermodynamics of adsorption deals with the transformation of substance and energy in systems as they advance to acquire a balanced condition [26]. In thermodynamic studies, the principles of normal enthalpy (ΔH°), standard free energy (ΔG°), and standard entropy (ΔS°) are necessary. The values of ΔH°, ΔS°, and ΔG° are obtained through the following equations:

$$\ln k_d = \frac{\Delta S}{R} - \frac{\Delta H}{RT} \quad (2)$$

$$\Delta G^\circ = \Delta H^\circ - T\Delta S^\circ \quad (3)$$

$$k_d = \frac{q_e}{C_e} \quad (4)$$

where q_e is the quantity of adsorbed Cr(VI) at an equilibrium state (mg/g) and C_e is the concentration of Cr (VI) after adsorption in solution (mg/L). The parameter of R (0/008314 J/mol) is the universal gas constant and T (°K) is the solution temperature. From the slope and intercept of the van't Hoff plot, we can find ΔH° and ΔS° (ln k_d vs. $1/T$), respectively.

3. Results and discussion

3.1. Characterization of the synthesized adsorbent

The XRD patterns of NPG, Fe_3O_4 nanoparticles and magnetite NPG are shown in Fig. 1(a). The intensity of NPG/Fe_3O_4 is shown in Fig. 1(b). The angle of the adsorbent is demonstrated in the range of 2θ = 5–80°, with the use of radiation Cu kα (λ = 1.5 Å). According to Fig. 1(a), the intense diffraction peaks at the Bragg angles of 30.09, 35.42, 37.05, 43.05, 53.39, 56.94, and 62.51 correspond to the (2 2 0), (3 1 1), (2 2 2), (4 0 0), (4 2 2), (5 1 1), and (4 4 0) facets of the cubic spinal crystal planes of Fe_3O_4 (JCPDS card No. 19-0629), respectively. The carbon peak is marked in the range of 25. Peaks aspects of nanoparticles (Fe_3O_4) on the absorbent structure are shown in the range between 45.5° and 55.6° [27].

The FT-IR spectra of synthesized composite of NPG, NPG/Fe_3O_4, and NPG/Fe_3O_4 with Cr(VI) are represented in Fig. 1(c). View of the magnetic nanoparticles at a wavelength of 582 cm^{-1} shows that the Fe–O bonds between groups are in the form of Tetrahedron [28]. The other groups that have emerged in the wavelength of 1,421.86 cm^{-1} represent aromatic C=C bonds and finally alkoxy CO bond is defined at the wavelength of 1,029 cm^{-1} [29].

The morphology, size, and surface area of NPG were analyzed by SEM in high magnification. Fig. 1(d) and (e) shows the good porosity and high adsorption

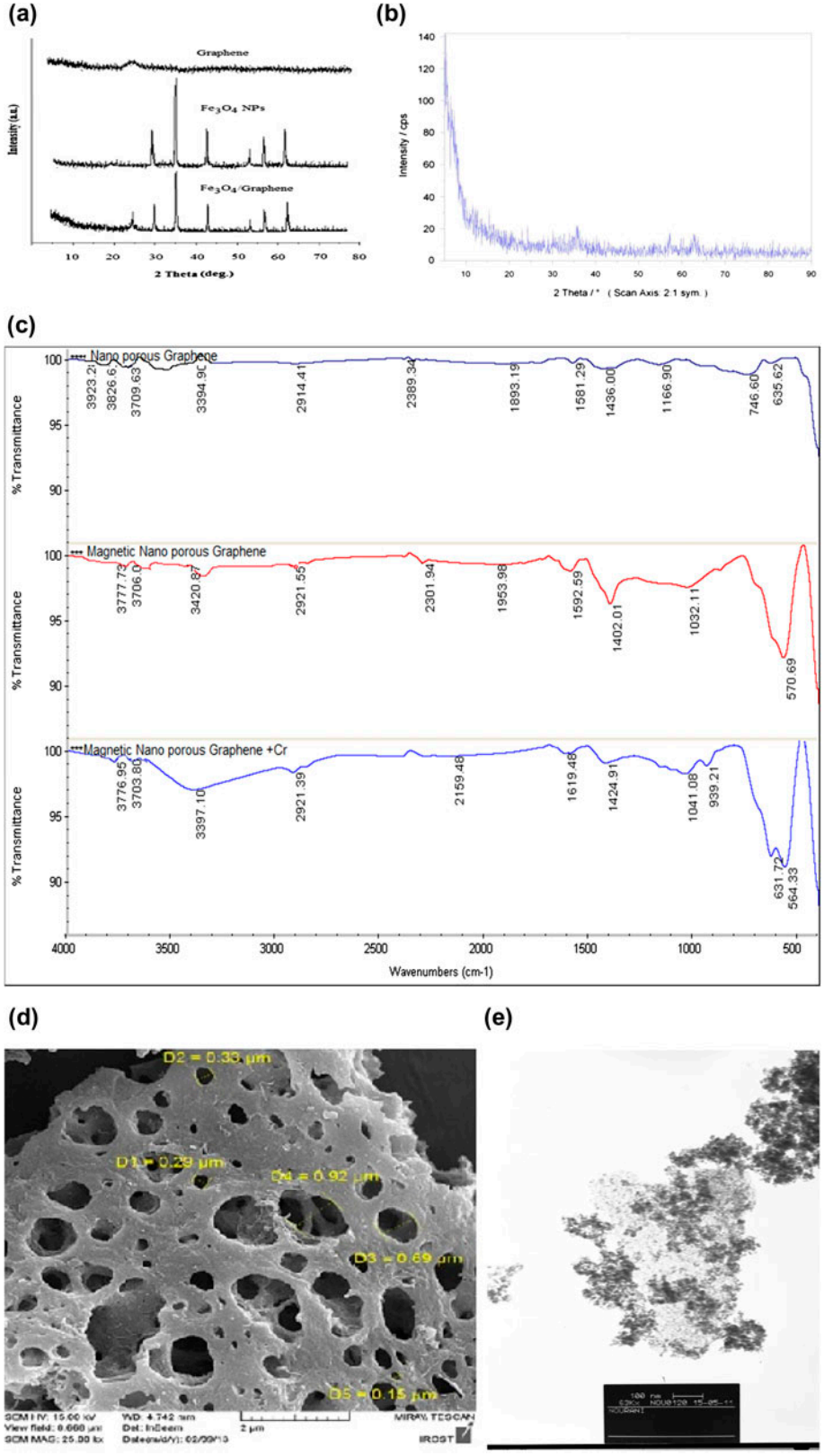

Fig. 1. Characterization of synthesized adsorbent, XRD analysis of graphene, Fe_3O_4 NPs, and NPG/Fe_3O_4 (a), XRD analysis of magnetic NPG (b), FT-IR spectra of synthesized adsorbent (c), SEM image of NPG (d), and TEM image of magnetic NPG in low-magnification (e).

capacity of NPG/Fe_3O_4. It should be pointed out that a high density of Fe_3O_4 nanoparticles is noticed on the NPG layers (Fig. 1(e)).

The surface area, pore size, and pore volume of NPG and Fe_3O_4 nanoparticles were measured using the BET analysis (Table 1). The results imply that the highest surface area of NPG and Fe_3O_4 nanoparticles was 850 and 93.5 $m^2\ g^{-1}$, respectively. This indicates that NPG adsorption capacity for contaminant is much higher than Fe_3O_4 nanoparticles. The specific surface area and pore volume of NPG were also larger than Fe_3O_4 nanoparticles.

3.2. Effect of solution pH

The effect of solution pH on heavy metals removal is one of the main parameters that plays an important role in controlling the adsorption process [30]. The amount of Cr(VI) removal in various ranges of pH (2, 3, 4, 5, 6, 7, 8, 9, 10) is shown in Fig. 2(a). It can be seen that the removal efficiency of Cr(VI) increased as a function of acidity of the solution. The maximum rate of adsorption is found at pH values ranging from 2 to 3 that is in accordance with the results of published data by many researchers [31]. Also in a similar study, pH 3 is an optimum pH value for the removal of Cr(VI) by nZVI-Fe_3O_4 nanocomposite and activated carbon [32]. The Cr(VI) speciation includes $Cr_2O_7^{2-}$, $HCrO_4^-$, $Cr_3O_{10}^{2-}V_2^-$ Cr_4O_{13}), that are having negative charges [33]. It is concluded that the reduction of Cr (VI) to Cr(III) at acidic conditions promotes the efficiency of the Cr(VI) removal, which was also suggested by the other researchers [34].

3.3. Effect of contact time

As shown in Fig. 2(b), it is evident that the adsorption of Cr(VI) onto the adsorbents at several reaction times (5, 15, 30, 60, 90, 120) increased until 60 min under the optimal conditions (pH 3, 200 rpm, $T = 25$°C and 0.035 g of absorbent). But, it reached at equilibrium state after 60 min. In other words, the time after 60 min, the availability of Cr(VI) adsorption to the active sites on the adsorbent surface is restricted. Karthik and Meenakshi reported that the adsorption of Cr(VI) by chitosan/polypyrrole composite reached the equilibrium state at 60 min [35].

3.4. Effect of adsorbent dosage

The effect of the optimal absorbent dosage on the Cr(VI) removal under optimal conditions (pH 3, $t = 60$ min, 200 rpm, $T = 25$°C) is shown in Fig. 3(a). It is evident that by increasing the absorbent dosage, the removal of Cr(VI) from aqueous solution was increased. Borhade and Uphade reported that the CdO and modified CdO nanoparticles were used for the removal of Cr(VI) by increasing the amount of adsorbent efficiency of adsorption increased but it remained constant after a 0.200 g/50 mL of adsorbent [36]. Results of the present study show that higher injection of adsorbents will not be effective in the removal of more dissolved Cr(VI).

3.5. Effect of initial Cr(VI) concentrations

The effect of various initial chromium concentrations (25, 50, 100 and 200 mg/L) under optimum conditions (pH 3, time = 60, 200 rpm, $T = 25$°C, $m_0 = 0.2$ g) is shown in Fig. 3(b). By increasing the initial concentration of dissolved Cr(VI), adsorption capacity was reduced. The main reason for this observation can be justified by limited pore size and active sites on the adsorbent surfaces [37].

3.6. Adsorption isotherms

Equilibrium adsorption isotherm models are used for better explanation of adsorbent capacity. The obtained values, based on the Langmuir and Freundlich models, for Cr(VI) sorption on NPG/Fe_3O_4 at ambient temperature and optimum conditions (pH 3, time = 60, 200 rpm, $m = 0.2$ g) are shown in Table 2(a).

The correlation coefficient (R^2) of the Freundlich isotherm is bigger than the Langmuir model. This result confirms that the Freundlich isotherm model is in good agreement with the experimental data in optimal conditions (25–200 mg/L of metal concentrations, pH of 3, the contact time of 60 min, adsorbent dosage of 0.035 g/L). The Freundlich model explains

Table 1
BET analysis of NPG

Sample	Surface area ($m^2\ g^{-1}$)	Pore size (Å)	Pore volume ($cm^3\ g^{-1}$)
NPG	850	99.5	2.11
Fe_3O_4 nanoparticle	93.5	–	2.37

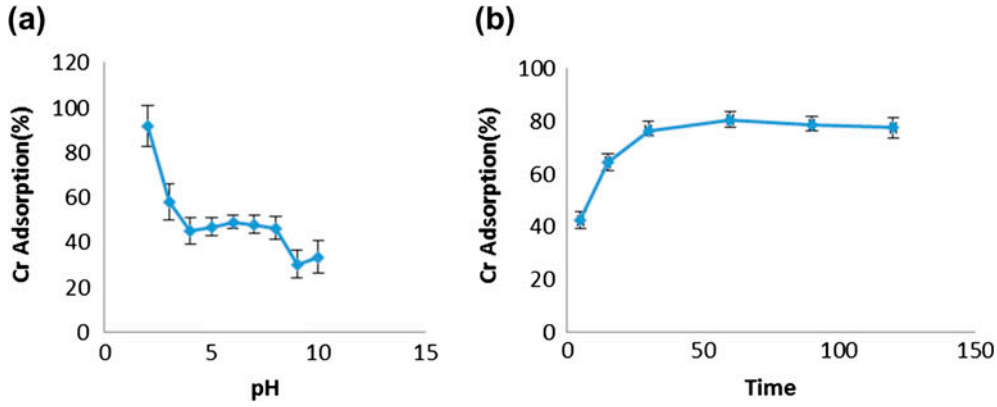

Fig. 2. Effects of pH (a) and contact time (b) on the Cr(VI) removal (pH 3, contact time = 60 min, 200 rpm, T = 25°C, m_0 = 0.2 g).

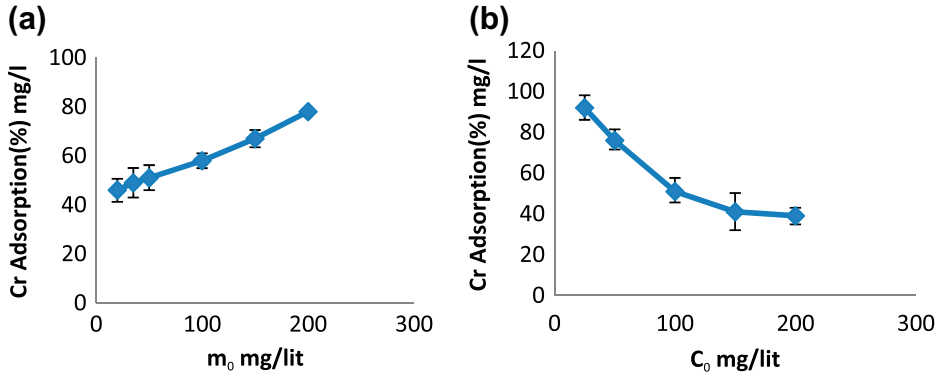

Fig. 3. Effects of adsorbent dose (a) and Cr(VI) concentrations (b) on the adsorption efficiency (pH 3, time = 60 min, 200 rpm, T = 25°C, m_0 = 0.2 g).

Table 2
The parameters of the adsorption isotherm models (a), the parameters of the adsorption kinetic models (b) in optimum conditions (pH 3, time = 60 min, 200 rpm, T = 25°C, m_0 = 0.2 g)

(a) Isotherm models	Parameters	
Langmuir	q_m(mg/g)	43.5
	k_L(L/mg)	0.048
	R_L	0.001
	R^2	0.89
Freundlich	k_F (mg/g(Lmg)/n)	4.49
	n	3.63
	R^2	0.97
(b) Kinetic models	Parameters	
Pseudo-first-order	$q_{e,cal}$ (mg/g)	2.806
	k_1 (min^{-1})	0.052
	R^2	0.942
Pseudo-second-order	$q_{e,cal}$ (mg/g)	23.923
	k_2 (g/mg)(min^{-1})	0.01
	R^2	0.99

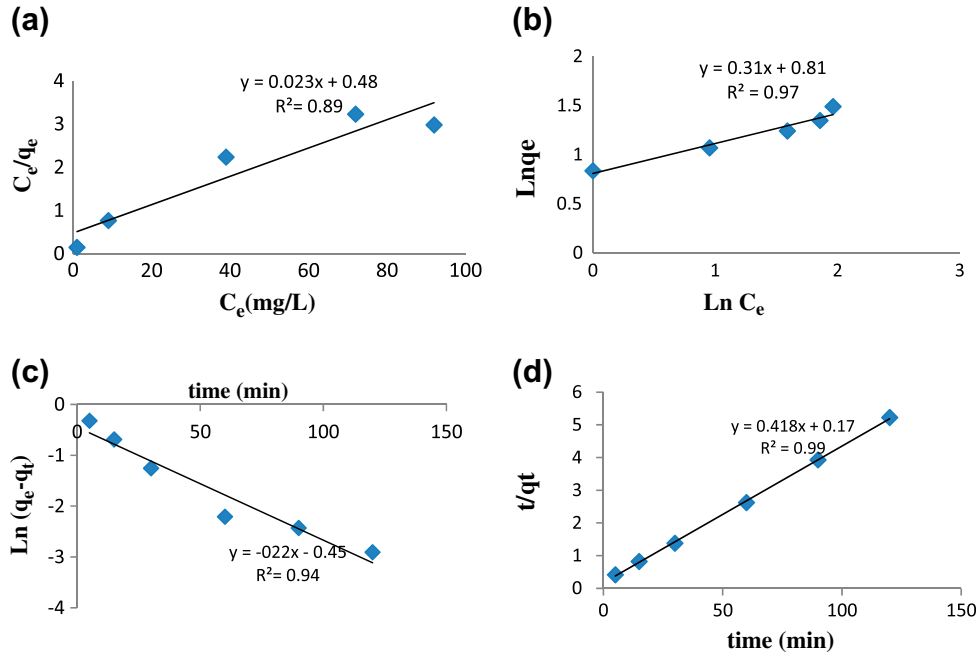

Fig. 4. The Langmuir (a), Freundlich (b) isotherm models and pseudo-first-order (c) and pseudo-second-order (d) kinetic models for the adsorption of Cr(VI) on NPG/Fe_3O_4 (pH 3, time = 60 min, 200 rpm, T = 25˚C, m_0 = 0.2 g).

adsorption on a heterogeneous surface with unequal energy and is not only restricted to the monolayer formation but also used for multilayer adsorption. It is also observed that the values of R_L lie between 0 and 1, indicating that Cr(VI) ions have been desirably adsorbed on NPG/Fe_3O_4. In Table 2(a), the rates of k_F and $1/n$ are computed from the intercept and slope of the plot of log q_e vs. log C_e, respectively. According to the obtained results, when the amount of k_F value increased, the adsorption capacity of the adsorbent was increased as well. It can be inferred that Cr(VI) adsorption on NPG/Fe_3O_4 at ambient temperature and optimal condition (pH 3, time = 60 min, 200 rpm, T = 25˚C, m = 0.2 g) represents beneficial adsorption, Ali Azari with the other associates in their research achieved similar results [38].

3.7. Kinetic study

The adsorption kinetic models of Cr(VI) on NPG/Fe_3O_4 along with their corresponding regression coefficients are given in Table 2(b). These are further verified by the curves presented in Fig. 4(c) and (d). According to the regression coefficient (R^2), the adsorption kinetics can be better explained by the pseudo-second-order model. Similar results were also reported by the other researchers that shown pseudo-second-order model fitted better the experimental data [39].

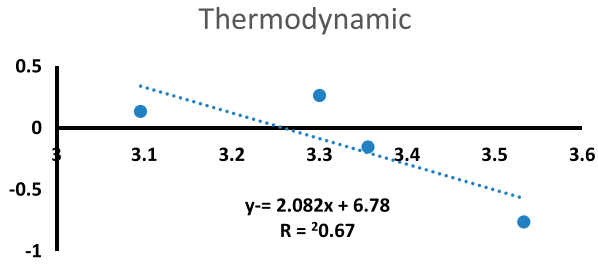

Fig. 5. Thermodynamic curve of Cr(VI) adsorption onto NPG/Fe_3O_4.

3.8. Thermodynamics of adsorption

The thermodynamic curve of Cr(VI) adsorption on NPG/Fe_3O_4 is demonstrated in Fig. 5. The results are confirmed by the curve where the values of ΔH° and ΔS° can be achieved from the slope and intercept of the plot of ln K° against $1/T$, respectively. The other computed parameters are recorded in Table 3. The negative ΔG° values pointed that the adsorption of Cr^{6+} on NPG/Fe_3O_4 is an endothermic and spontaneous process. The positive value of ΔH° recommends that the adsorption process is endothermic [40]. The amount of ΔS° is also positive, which describes adsorption process is spontaneous with high affinity. It also advises that there are little structural changes in both adsorbate and adsorbent [33]. The obtained q_m

Table 3
Thermodynamic parameters of Cr(VI) adsorption on NPG/Fe_3O_4 adsorbent (pH 3, time = 60 min, 200 rpm, T = 25°C, m_0 = 0.2 g)

Temperature (°K)	ln k_d	ΔG° (kJ/mol)	ΔH° (kJ/mol)	ΔS° (kJ/mol K)
283	−0.308	−79.374	17.31	0.06
298	0.133	−87.875		
303	0.263	−90.810		
323	0.133	−103.24		

Table 4
Comparison of adsorption capacity of Cr(VI) among different adsorbents documented in the literature

Adsorbent	pH	Temperature (°C)	Isotherms	Kinetic	q_m	Refs.
MWCNT/Fe_3O_4	2	45	Langmuir	Pseudo-second-order	76.92	[41]
Neem sawdust and Mango sawdust	2	25	Freundlich	Pseudo-second-order	37.73 58.82	[42]
Arachis hypogeal shell in the form of beads(AHSB)	2	25	Langmuir	Pseudo-second-order	6	[43]
Chitosan flaskes	–	25	Langmuir	Pseudo-second-order	22.09	[44]
Larch tannin resin (LTNI)	1	25	Langmuir	Pseudo-second-order	9.13	[45]
Treated sawdust of Sal tree	3.5	–	Langmuir	Pseudo-second-order	9.55	[46]
NPG/Fe_3O_4	3	30	Freundlich	Pseudo-second-order	43.5	This study

of the NPG/Fe_3O_4 was compared with the other adsorbents on the Cr(VI) removal as shown in Table 4.

4. Conclusion

NPG was prepared by CVD technique that is magnetized by Fe_3O_4 and Fe_2O_3 powder (NPG/Fe_3O_4) for feasible separation from water. Through a chemical deposition method, magnetic iron oxide (nano-sized) was homogeneously dispersed onto NPG layers. In addition, XRD, FTIR, TEM, SEM, and BET techniques were used as various measurement tools for characterization of NPG/Fe_3O_4. These adsorbents are used for the Cr(VI) removal from aqueous solutions in a batch adsorption process and at optimum conditions. The optimum conditions for the adsorption process obtained at low acidity (pH 3), the contact time of 60 min, the temperature of 30°C, 200 rpm, and 0.2 g of adsorbent dosage. The results showed that NPG/Fe_3O_4 had a great potential to be used as an effective absorbent for removing Cr(VI) from solution. The equilibrium data were applied to describe adsorption process that is better fitted to the Freundlich isotherm model. Kinetic data adsorption can be best described by a pseudo-second-order kinetic model. The sorption reaction is an endothermic and spontaneous process in nature. Ultimately, from the findings of this study, it can be outlined that NPG/Fe_3O_4 can be applied as a feasible and promising adsorbent in the purification of water and wastewaters. It is also an environmentally friendly technique that does not leave any adverse effect on aquatic environment.

Acknowledgments

The authors are grateful for the support received from the Research Institute of Tehran Petroleum Industry. We express particular appreciation to Babak Kakavandi and Masoud Moradi for their assistance.

References

[1] M. Kobya, Removal of Cr(VI) from aqueous solutions by adsorption onto hazelnut shell activated carbon: Kinetic and equilibrium studies, Bioresour. Technol. 91 (2004) 317–321.
[2] X. Guo, G.T. Fei, H. Su, L. De Zhang, High-performance and reproducible polyaniline nanowire/tubes for removal of Cr(VI) in aqueous solution, J. Phys. Chem. C 115 (2011) 1608–1613.

[3] M. Moradi, L. Hemati, M. Pirsaheb, K. Sharafi, Removal of hexavalent chromium from aqueous solution by powdered scoria-equilibrium isotherms and kinetic studies, World Appl. Sci. J. 33 (2015) 393–400.
[4] B. Mukhopadhyay, J. Sundquist, R.J. Schmitz, Removal of Cr(VI) from Cr-contaminated groundwater through electrochemical addition of Fe(II), J. Environ. Manage. 82 (2007) 66–76.
[5] S.T. Farrell, C.B. Breslin, Reduction of Cr(VI) at a polyaniline film: Influence of film thickness and oxidation state, Environ. Sci. Technol. 38 (2004) 4671–4676.
[6] S. Chakraborty, J. Dasgupta, U. Farooq, J. Sikder, E. Drioli, S. Curcio, Experimental analysis, modeling and optimization of chromium(VI) removal from aqueous solutions by polymer-enhanced ultrafiltration, J. Membr. Sci. 456 (2014) 139–154.
[7] S. Chen, Q. Yue, B. Gao, X. Xu, Equilibrium and kinetic adsorption study of the adsorptive removal of Cr(VI) using modified wheat residue, J. Colloid Interface Sci. 349 (2010) 256–264.
[8] A. Daifullah, S. Yakout, S. Elreefy, Adsorption of fluoride in aqueous solutions using $KMnO_4$-modified activated carbon derived from steam pyrolysis of rice straw, J. Hazard. Mater. 147 (2007) 633–643.
[9] T. Wu, X. Cai, S. Tan, H. Li, J. Liu, W. Yang, Adsorption characteristics of acrylonitrile, p-toluenesulfonic acid, 1-naphthalenesulfonic acid and methyl blue on graphene in aqueous solutions, Chem. Eng. J. 173 (2011) 144–149.
[10] C. Balan, I. Volf, D. Bilba, Chromium(VI) removal from aqueous solutions by purolite base anion-exchange resins with gel structure, Chem. Ind. Chem. Eng. Q. 19 (2013) 615–628.
[11] X.-J. Hu, J.-S. Wang, Y.-G. Liu, X. Li, G.-M. Zeng, Z.-L. Bao, X.-X. Zeng, A.-W. Chen, F. Long, Adsorption of chromium(VI) by ethylenediamine-modified cross-linked magnetic chitosan resin: Isotherms, kinetics and thermodynamics, J. Hazard. Mater. 185 (2011) 306–314.
[12] E. Rosales, M. Pazos, M.A. Sanromán, Advances in the electro-fenton process for remediation of recalcitrant organic compounds, Chem. Eng. Technol 35 (2012) 609–617.
[13] M. Aliabadi, I. Khazaei, H. Fakhraee, M. Mousavian, Hexavalent chromium removal from aqueous solutions by using low-cost biological wastes: Equilibrium and kinetic studies, Int. J. Environ. Sci. Technol. 9 (2012) 319–326.
[14] J. Yan, T. Wei, W. Qiao, B. Shao, Q. Zhao, L. Zhang, Z. Fan, Rapid microwave-assisted synthesis of graphene nanosheet/Co_3O_4 composite for supercapacitors, Electrochim. Acta 55 (2010) 6973–6978.
[15] Y. Zhu, S. Murali, W. Cai, X. Li, J.W. Suk, J.R. Potts, R.S. Ruoff, Graphene and graphene oxide: Synthesis, properties, and applications, Adv. Mater. 22 (2010) 3906–3924.
[16] B. Kakavandi, A. Esrafili, A. Mohseni-Bandpi, J.A. Jonidi, K.R. Rezaei, Magnetic Fe_3O_4@ C nanoparticles as adsorbents for removal of amoxicillin from aqueous solution, Water Sci. Technol. 69(1) (2014) 147–155.
[17] J. Li, S. Zhang, C. Chen, G. Zhao, X. Yang, J. Li, X. Wang, Removal of Cu(II) and fulvic acid by graphene oxide nanosheets decorated with Fe_3O_4 nanoparticles, ACS Appl. Mater. Interfaces 4 (2012) 4991–5000.
[18] S. Shariati, M. Faraji, Y. Yamini, A.A. Rajabi, Fe_3O_4 magnetic nanoparticles modified with sodium dodecyl sulfate for removal of safranin O dye from aqueous solutions, Desalination 270 (2011) 160–165.
[19] R. Muñoz, C. Gómez-Aleixandre, Review of CVD synthesis of graphene, Chem. Vap. Deposition 19 (2013) 297–322.
[20] X. Li, W. Cai, J. An, S. Kim, J. Nah, D. Yang, R. Piner, A. Velamakanni, I. Jung, E. Tutuc, Large-area synthesis of high-quality and uniform graphene films on copper foils, Science 324 (2009) 1312–1314.
[21] A. Reina, X. Jia, J. Ho, D. Nezich, H. Son, V. Bulovic, M.S. Dresselhaus, J. Kong, Layer area, few-layer graphene films on arbitrary substrates by chemical vapor deposition, Nano Lett. 9 (2009) 3087–3087.
[22] S. Bae, H. Kim, Y. Lee, X. Xu, J.-S. Park, Y. Zheng, J. Balakrishnan, T. Lei, H.R. Kim, Y.I. Song, Roll-to-roll production of 30-inch graphene films for transparent electrodes, Nat. Nanotechnol. 5 (2010) 574–578.
[23] S. Pourmand, M. Abdouss, A. Rashidi, Fabrication of nanoporous graphene by chemical vapor deposition (CVD) and its application in oil spill removal as a recyclable nanosorbent, J. Ind. Eng. Chem. 22 (2015) 8–18.
[24] Z.-Y. Juang, C.-Y. Wu, A.-Y. Lu, C.-Y. Su, K.-C. Leou, F.-R. Chen, C.-H. Tsai, Graphene synthesis by chemical vapor deposition and transfer by a roll-to-roll process, Carbon 48 (2010) 3169–3174.
[25] B. Li, H. Cao, J. Shao, G. Li, M. Qu, G. Yin, Co_3O_4@ graphene composites as anode materials for high-performance lithium ion batteries, Inorg. Chem. 50 (2011) 1628–1632.
[26] B. Kakavandi, R.R. Kalantary, A. Esrafily, A.J. Jafari, A. Azari, Isotherm, kinetic and thermodynamic of reactive Blue 5 (RB5) dye adsorption using Fe_3O_4 nanoparticles and activated carbon magnetic composite, J. Color Sci. Technol. 7 (2013) 237–248.
[27] R.R. Kalantary, A. Azari, A. Esrafili, K. Yaghmaeian, M. Moradi, K. Sharafi, The survey of Malathion removal using magnetic graphene oxide nanocomposite as a novel adsorbent: Thermodynamics, isotherms, and kinetic study, Desalin. Water Treat. (2015) 1–14.
[28] A.Z.M. Badruddoza, Z.B.Z. Shawon, W.J.D. Tay, K. Hidajat, M.S. Uddin, Fe_3O_4/cyclodextrin polymer nanocomposites for selective heavy metals removal from industrial wastewater, Carbohydr. Polym. 91 (2013) 322–332.
[29] Z. Ji, X. Shen, Y. Song, G. Zhu, In situ synthesis of graphene/cobalt nanocomposites and their magnetic properties, Mater. Sci. Eng. B 176 (2011) 711–715.
[30] H.-H. Cho, K. Wepasnick, B.A. Smith, F.K. Bangash, D.H. Fairbrother, W.P. Ball, Sorption of aqueous Zn[II] and Cd[II] by multiwall carbon nanotubes: The relative roles of oxygen-containing functional groups and graphenic carbon, Langmuir 26 (2009) 967–981.
[31] S.-M. Lee, W.-G. Kim, C. Laldawngliana, D. Tiwari, Removal behavior of surface modified sand for Cd(II) and Cr(VI) from aqueous solutions, J. Chem. Eng. Data 55 (2010) 3089–3094.
[32] F.A. Ihsanullah, B. Al-Khaldi, A.M. Abu-Sharkh, M.I. Abulkibash, T. Qureshi, M.A. Laoui, Atieh, Effect of acid modification on adsorption of hexavalent chromium(Cr(VI)) from aqueous solution by activated carbon and carbon nanotubes, Desalin. Water Treat. 57 (2015) 1–13.

[33] K. Selvi, S. Pattabhi, K. Kadirvelu, Removal of Cr(VI) from aqueous solution by adsorption onto activated carbon, Bioresour. Technol. 80 (2001) 87–89.
[34] L. Wu, L. Liao, G. Lv, F. Qin, Y. He, X. Wang, Micro-electrolysis of Cr(VI) in the nanoscale zero-valent iron loaded activated carbon, J. Hazard. Mater. 254–255 (2013) 277–283.
[35] R. Karthik, S. Meenakshi, Removal of hexavalent chromium ions from aqueous solution using chitosan/polypyrrole composite, Desalin. Water Treat. 56 (2014) 1–14.
[36] A.V. Borhade, B.K. Uphade, Removal of chromium (VI) from aqueous solution using modified CdO nanoparticles, Desalin. Water Treat. 57 (2015) 1–13.
[37] R. Rezaei Kalantry, A. Jonidi Jafari, A. Esrafili B. Kakavandi, A. Gholizadeh, A. Azari, Optimization and evaluation of reactive dye adsorption on magnetic composite of activated carbon and iron oxide, Desalin. Water Treat. 57 (2015) 1–12.
[38] A. Mohseni-Bandpi, B. Kakavandi, R.R. Kalantary, A. Azari, A. Keramati, Development of a novel magnetite–chitosan composite for the removal of fluoride from drinking water: Adsorption modeling and optimization, RSC Adv. 5 (2015) 73279–73289.
[39] B. Kakavandi, R.R. Kalantary, A.J. Jafari, S. Nasseri, A. Ameri, A. Esrafili, A. Azari, Pb(II) adsorption onto a magnetic composite of activated carbon and superparamagnetic Fe_3O_4 nanoparticles: Experimental and modeling study, CLEAN–Soil Air Water 43 (2015) 1157–1166.
[40] J. Xu, L. Wang, Y. Zhu, Decontamination of bisphenol A from aqueous solution by graphene adsorption, Langmuir 28 (2012) 8418–8425.
[41] R. Ghasemi, T. Sayahi, S. Tourani, M. Kavianimehr, 40 Modified magnetite nanoparticles for hexavalent chromium removal from water, Desalin. Water Treat. 37(9) (2016) 1303–1314.
[42] V. Vinodhini, N. Das, Relevant approach to assess the performance of sawdust as adsorbent of chromium (VI) ions from aqueous solutions, Int. J. Environ. Sci. Technol. 7 (2010) 85–92.
[43] G. Mahajan, D. Sud, Kinetics and equilibrium studies of Cr(VI) metal ion remediation by Arachis hypogea shells: A green approach, BioResources 6 (2011) 3324–3338.
[44] Y.A. Aydın, N.D. Aksoy, Adsorption of chromium on chitosan: Optimization, kinetics and thermodynamics, Chemical Eng. J. (Lausanne, Switzerland: 1996), 151 (2009) 188–194.
[45] Z. Huang, B. Zhang, G. Fang, Adsorption behavior of Cr(VI) from aqueous solutions by microwave modified porous larch tannin resin, BioResources 8 (2013) 4593–4608.
[46] S.S. Baral, S.N. Das, P. Rath, Hexavalent chromium removal from aqueous solution by adsorption on treated sawdust, Biochem. Eng. J. 31 (2006) 216–222.